Recent B Results from the CLEO Collaboration

A. P. Freyberger
University of Florida, Gainsville, FL 32611
Representing the CLEO Collaboration

November 18, 1992

Abstract

Recent results from the CLEO collaboration in Charm and Beauty decays are presented. Results of a search for the radiative decay of the D^{*+} meson are presented, as well as a remeasurement of the D^* branching ratios. Preliminary results on rare B decays are also presented as well as a preliminary results on the semileptonic B^+ and B^0 inclusive branching ratios.

1 Introduction

The local interest in building a so called *B factory* here at SLAC, and from where I came from, Cornell University, compels me to discuss measurements made recently with the CLEO-II detector in the CESR storage ring, that are not only interesting for the intrinsic physics content but may have an impact on future B-factory designs. Since the CLEO-II detector was commissioned in the fall of 1989, over $1 fb^{-1}$ of $\Upsilon(4S)$ data has been recorded, corresponding to over one million $B\overline{B}$ decays. This has been a direct result of the superb performance of the CESR storage ring, which now operates with a peak luminosity of $2.5 * 10^{32} cm^{-2} sec^{-1}$. The CLEO-II detector records approximately $7.5 pb^{-1}$ of data on a typical day, with a peak day of $10.5 pb^{-1}$. The large data set coupled with an excellent detector provides us with sensitivity approaching theoretical expectations in many rare decay modes.

© A. P. Freyberger 1993

2 The CLEO-II detector

The cylindrical 4π CLEO-II detector consists of central tracking detectors, time-of-flight scintillators, and an electromagnetic calorimeter immersed within a 1.5 Tesla magnetic field. Outside of the magnetic field lays a sandwich of ranging steel and proportional detectors. A detailed description of the CLEO II detector can be found elsewhere [1].

The tracking detectors and CsI calorimeter provide excellent efficiency and resolution for charged tracks and photons. The charged particle momentum resolution is measured to be

$$(\frac{\delta p}{p})^2 = (0.0015p)^2 + (0.005)^2 \quad p \; in \; GeV/c, \tag{1}$$

and the energy resolution of the calorimeter is measured to be

$$\frac{\sigma(E)}{E}(\%) = \frac{0.35}{E^{(0.75)}} + 1.9 - 0.1E \quad E \; in \; GeV. \tag{2}$$

The fact that CLEO-II detects neutrals with efficiency and resolution comparable to the charged particle system has been a great advantage in reconstructing processes that include γ's or π^0's in the final state.

3 Remeasurement of the D* branching ratios

Although the branching fractions for the five possible decay modes of the D^{*+} and D^{*0} have been measured by several experiments [2-3], the decay mode, $D^{*+} \to D^+\gamma$ has not been directly observed. Using the exceptional resolution and efficiency of the CsI calorimeter, we attempt to observe for the first time the radiative decay of the D^{*+}. In the process we obtain new measurements for all the D^* branching ratios [4]. This analysis is based in $780\,\mathrm{pb}^{-1}$ of continuum and resonance data.

3.1 $\mathcal{B}(D^{*0} \to D^0\pi^0)$ and $\mathcal{B}(D^{*0} \to D^0\gamma)$

Since the sum of the $\mathcal{B}(D^{*0} \to D^0\pi^0)$ and $\mathcal{B}(D^{*0} \to D^0\gamma)$ must sum to unity, the ratio $\frac{\mathcal{B}(D^{*0}\to D^0\gamma)}{\mathcal{B}(D^{*0}\to D^0\pi^0)}$ determines the absolute branching fractions for the two decay channels. For both modes we use the $D^0 \to K^-\pi^+$ decay channel so that systematics in reconstructing the D^0 cancel in the ratio. All di-photon combinations within 3.0σ ($\sigma_{\pi^0} = 5MeV/c^2$) of the known π^0 mass ($0.135MeV/c^2$) are selected as π^0 candidates. We require each of the photons to be in the barrel portion of the calorimeter, $|cos(\theta_\gamma)| \leq 0.71$. We then kinematically

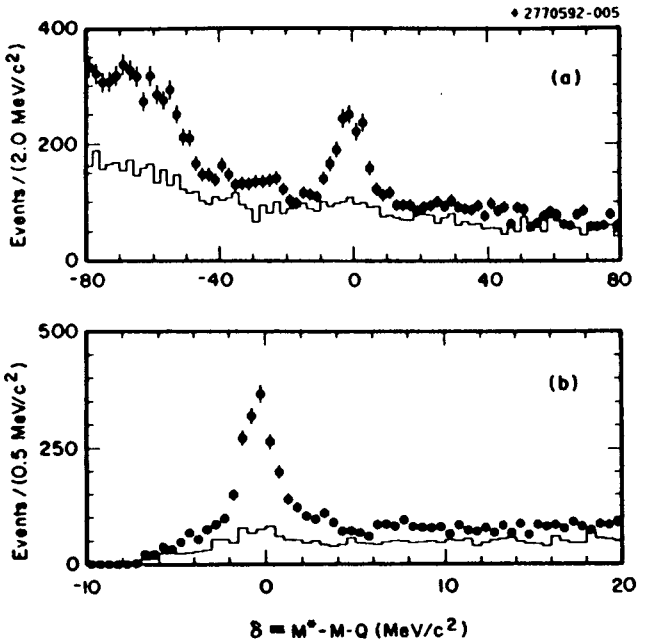

Figure 1: Mass difference distributions for (a) $D^{*0} \to D^0\gamma$ combinations and (b) $D^{*0} \to D^0\pi^0$ combinations. The points are for mass difference candidates for D^0 candidates within the D signal region while the histogram represents fake D^0 candidates by using sidebands in D^0 mass.

constrain the γ four vectors to the known π^0 mass. For the electromagnetic transition we require that the photon be incident in the barrel portion of the calorimeter and that it be forward with respect to the D^{*0} laboratory momentum in the D^{*0} center-of-mass. This cut reduces the soft photon background. Combinatoric background is also reduced by requiring that the D^{*0} have a large fraction of the available momentum, $x_{D^{*0}} = p_{D^{*0}}/p_{max} > 0.5$. Figure 1 shows the mass difference, $\delta = M_{D^{*0}} - M_{D^0} - Q$, for the two-decay channels. The solid points represent the signal and the histogram is from D^0 mass sidebands.

In addition to the two yields we need the relative efficiency $\frac{\epsilon_{\pi^0}}{\epsilon_\gamma}$. We determine the ratio of efficiencies via a full GEANT simulation of the detector [5]. We assign a systematic error of 5% on the efficiency ratio by studying the

Decay Mode	Branching Fraction	
	CLEO II (%)	PDB[7] (%)
$D^{*+} \to D^+\gamma$	$1.1 \pm 1.4 \pm 1.5$	18 ± 4
$D^{*+} \to D^+\pi^0$	$31.0 \pm 0.5 \pm 0.7$	27.1 ± 2.5
$D^{*+} \to D^0\pi^+$	$67.9 \pm 1.1 \pm 2.0$	55 ± 4
$D^{*0} \to D^0\gamma$	$36.5 \pm 2.3 \pm 3.5$	45 ± 6
$D^{*0} \to D^0\pi^0$	$63.5 \pm 2.3 \pm 3.5$	55 ± 6

Table 1: Branching ratios for D^* decays.

ratio $\frac{\mathcal{B}(\eta \to \pi^0\pi^0\pi^0)}{\mathcal{B}(\eta \to \gamma\gamma)}$. The values obtain for the D^{*0} branching ratios are in Table 1.

3.2 $\mathcal{B}(D^{*+} \to D^+\pi^0)$, $\mathcal{B}(D^{*+} \to D^+\gamma)$ and $\mathcal{B}(D^{*+} \to D^0\pi^+)$

Determining the D^{*+} branching fractions is complicated by the fact that there are three available channels. However isospin and phase space fix the ratio of $\frac{\mathcal{B}(D^{*+} \to D^0\pi^+)}{\mathcal{B}(D^{*+} \to D^+\pi^0)}$ to 2.19 ± 0.17 [6]. With this constraint we need only to measure the ratio of $\frac{\mathcal{B}(D^{*+} \to D^+\gamma)}{\mathcal{B}(D^{*+} \to D^+\pi^0)}$ to determine all three branching ratios. The analysis proceeds as in the D^{*0} case, only now we reconstruct $D^+ \to K^-\pi^+\pi^+$. We cut harder on the momentum fraction of the D^{*+}, $x_{D^{*+}} > 0.7$, to further reduce the combinatoric background and provide increased sensitivity to the electromagnetic transition.

Figure 2 shows the mass difference plots for the two decay channels. The dashed histogram in Fig. (2a) is the signal distribution for $D^{*+} \to D^+\gamma$, while the solid histogram represents background from D^+ mass sidebands. The solid points are described below. Figure (2a) shows an enhancement in the signal region, however there is a known background due to $D_s^* \to D_s^+\gamma$ transitions. This feed down occurs when D_s^+ decays into three charged tracks that happen to fall in the D^+ mass region when combined as $K^-\pi^+\pi^+$. To eliminate some of this background we reject mass combinations consistent with $D_s^+ \to \Phi\pi^+$ or $D_s^+ \to \overline{K^*}K^+$ hypothesis. This veto rejects approximately 73% of the D_s^{*+} decays and retains 84% of the true D^{*+} decays. The background subtracted signal is shown as the solid points in Fig. (2a) Using the yields from the mass difference plots we obtain the branching ratios listed in Table 1.

The value measured for $D^{*+} \to D^+\gamma$ is significantly lower than previous measured values for this decay. This new small value for $D^{*+} \to D^+\gamma$ eliminates the need for an anomalously large charm quark magnetic moment necessary for the previously large values of $D^{*+} \to D^+\gamma$. We use the mea-

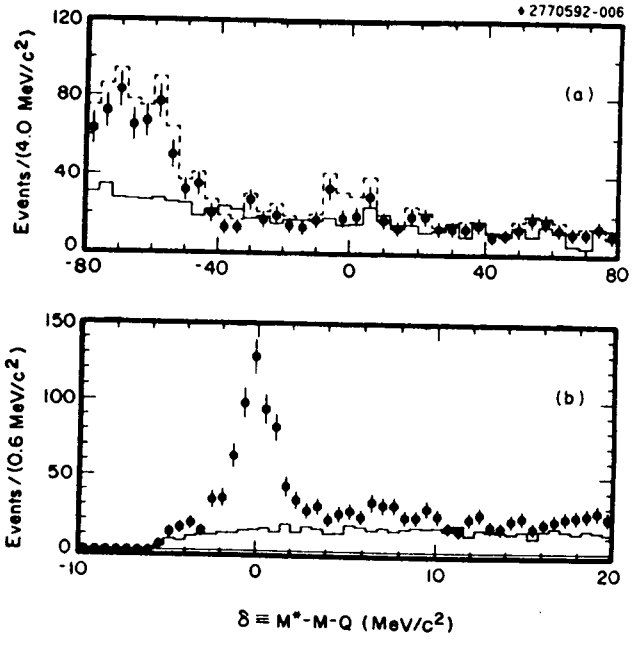

Figure 2: Mass difference distributions for (a) $D^{*+} \to D^+\gamma$ combinations and (b) $D^{*+} \to D^+\pi^0$ combinations. The points are for mass difference candidates for D^+ candidates within the D signal region while the histogram represents fake D^+ candidates by using sidebands in D^0 mass. The dashed histogram in (a) is the $D^{*+} \to D^+\gamma$ signal before subtracted feed down from $D_s^{*+} \to D_s^+\gamma$ decays.

surement to place an upper limit on the decay $D^{*+} \to D^+\gamma$ of 4.2% at the 90% confidence level. The new values for the D^* branching ratios will effect any previous exclusive measurement of $B \to D^*X$, specifically the change in the $D^{*+} \to D^0\pi^+$ will scale all $B \to D^{*+}X$ branching ratios by a factor of 0.81. The increase precision of the CLEO-II measurements of the D^* branching ratios will also aid in reducing systematic errors in B branching ratios that involve these channels.

4 Searches for rare B decays

CLEO presently has the largest data set of $B\overline{B}$ pairs recorded in e^+e^- interactions (over 10^6 $B\overline{B}$ events on tape). Although hadronic cross sections for b-quark production are two orders of magnitude larger than the cross section for $e+e^- \to \Upsilon(4S)$, the luminosity of the CESR storage ring gives CLEO better sensitivity to rare two-body B decays than any other current machine. In addition to the large data set, the cleanliness of the e^+e^- environment coupled with efficient charged particle tracking and neutral detection enables CLEO to set limits for rare decay modes approaching theoretical predictions. CLEO also benefits from the constraint that the B meson must have energy equal to that of the beam energy, this allows the calculation of the *beam constraint mass*. The B mass is calculated as follows

$$M_B^2 = E_{beam}^2 - (\sum \vec{P}_i)^2. \qquad (3)$$

The energy constraint reduces the width of the B mass by an order of magnitude, thus aiding background discrimination.

In this section I will present results on searches for the CP eigenstate, $B^0 \to \psi K^0$, $B^0 \to \psi K^{*0}$, and $B^0 \to \pi^+\pi^-$. Because these decay modes are CP eigenstate, knowledge of their decay rates is of interest to B-factory designers. Results will also be presented for an inclusive search for $b \to s\gamma$ decays, which, if observed, would be evidence for an electromagnetic penguin decay of the B^0 meson.

4.1 $B \to \psi K^{(*)}$

Current measurements of branching ratio of $B^0 \to K_s^0\psi$ indicate that approximately 10^8 $B^0\overline{B^0}$ events are needed to observe CP violation in the B system. Additional CP eigenstates of the B^0 meson can aid in reducing the estimated luminosity requirements. One such state is $B^0 \to \psi K^{*0}$. The decay $B^0 \to \psi K^{*0}$ is complicated by the fact that the CP of the final state depends on the angular momentum of the final state. The final state has *even* CP

Decay Mode	Events	Efficiency (incl. BR)(%)	Branching Ratio (%)
$B^- \to \psi K^-$	43 ± 6.7	4.5 ± 0.20	$0.102 \pm 0.016 \pm 0.013$
$B^0 \to \psi K^0$	6 ± 2.4	0.61 ± 0.02	$0.102 \pm 0.043 \pm 0.017$
$B^0 \to \psi K^{*0}$	28.5 ± 5.3	2.08 ± 0.10	$0.147 \pm 0.028 \pm 0.025$
$B^- \to \psi K^{*-}$	10 ± 3.2	0.60 ± 0.04	$0.178 \pm 0.056 \pm 0.026$

Table 2: Exclusive $B \to \psi K^{(*)}$ results.

when the orbital angular momentum, L, is 0 or 2, and has *odd* CP for L=1. If any one of these angular momentum states dominates the final state, then this mode can be used for CP violation studies. If the final state is a mixture of angular momentum states all is not lost, as a detailed moments analysis can be done to separate out the different CP eigenstates [8].

In this section new measurements of the branching ratio of $B^- \to \psi K^-$ and $B^0 \to \psi K^0$ will be presented. Measurements of $\mathcal{B}(B^0 \to \psi K^{*0}), K^{*0} \to K^-\pi^+$ and $\mathcal{B}(B^- \to \psi K^{*-}), K^{*-} \to K^-\pi^0$ will also be presented along with a measurement of the polarization in the $B \to \psi K^*$ decays. ψ's are reconstructed in the e^+e^- channel and the $\mu^+\mu^-$ channel. Figure 3 shows the inclusive ψ yield for the two dilepton channels in $923\,\mathrm{pb}^{-1}$ of data collected at the $\Upsilon(4S)$ resonance.

The ψ's are then combined with K's and K^*'s to form B candidates. Figure 4 shows the beam constrained mass for the four $B \to \psi K^{(*)}$ modes. The yields, efficiency and measured branching ratios are tabulated in Table 2.

Using isospin symmetry we can combine these results to obtain

$$\frac{\mathcal{B}(B \to \psi K^*)}{\mathcal{B}(B \to \psi K)} = 1.52 \pm 0.43 \qquad . \qquad (4)$$

This ratio is in agreement with the prediction from the BSW model of 1.61 [9].

4.1.1 Polarization measurements of $B \to \psi K^*$

In addition to the $B \to \psi K^*$ branching ratio, we measure the polarization of the ψK^* angular decay distributions. Integrating over χ, the angle between the ψ and K^* decay planes, we can write the decay angular distributions as

$$\frac{d^2\Gamma}{dcos\Theta_\psi dcos\Theta_{K^*}} \propto \frac{1}{4} sin^2\Theta_{K^*}(1+cos^2\Theta_\psi)(|H_{+1}|^2+|H_{-1}|^2)+cos^2\Theta_{K^*}sin^2\Theta_\psi|H_0|^2, \qquad (5)$$

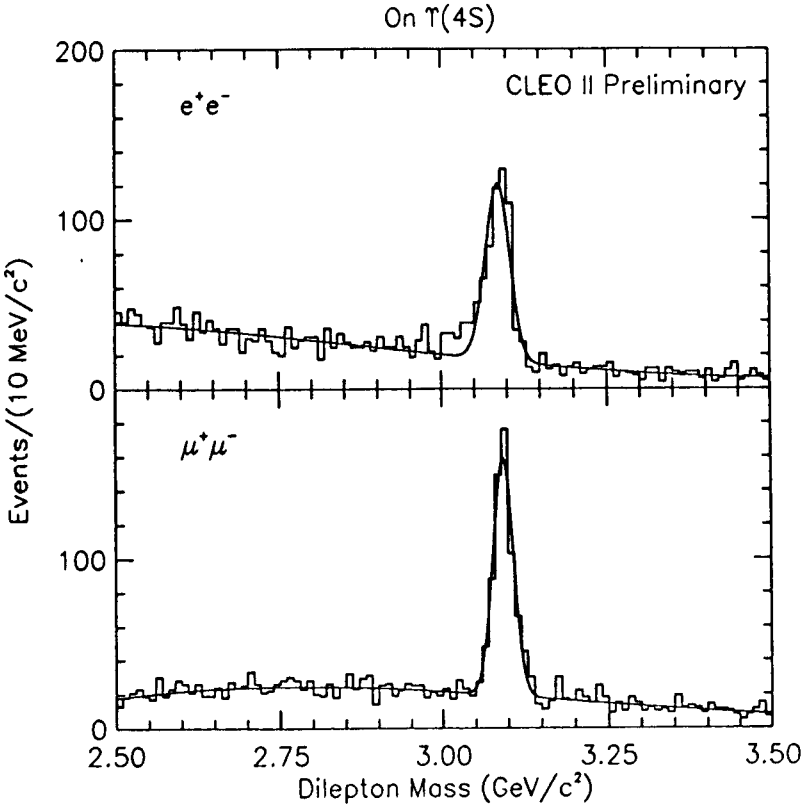

Figure 3: Invariant dilepton mass for ψ candidates. The top plot is for e^+e^- combinations and the bottom plot is $\mu^+\mu^-$ combinations.

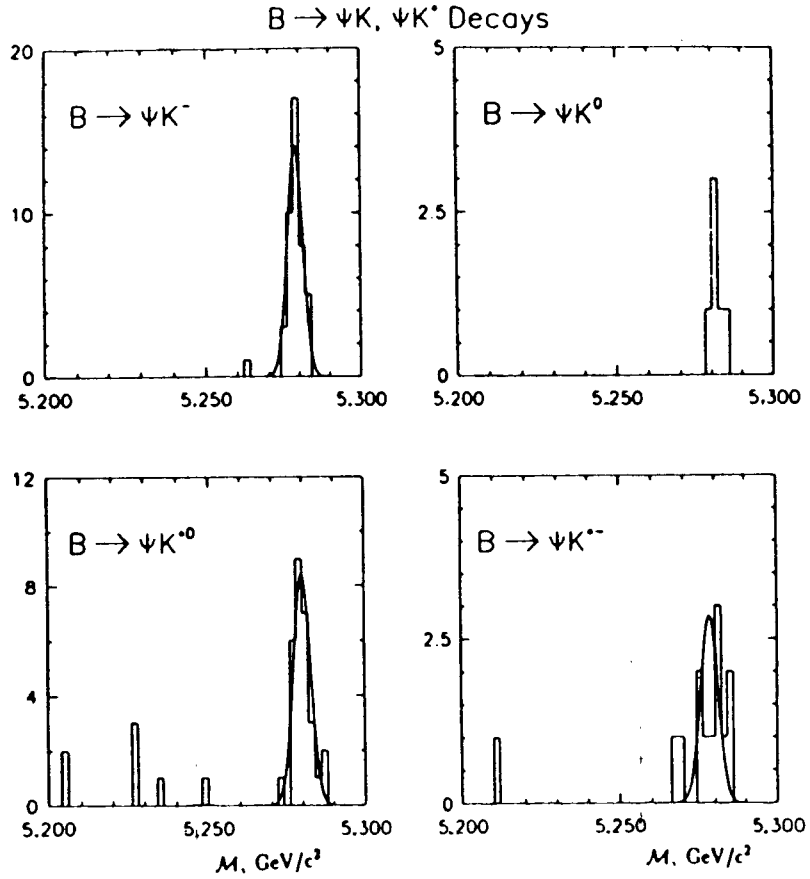

Figure 4: Beam constrained mass for a) $B^- \to \psi K^-$, b) $\overline{B^0} \to \psi \overline{K^0}$, c) $\overline{B^0} \to \psi \overline{K^{*0}}$, and d) $B^- \to \psi K^{*-}$.

with Θ_ψ defined as the angle between the lepton direction in the ψ rest frame and the ψ direction in the B rest frame, and Θ_{K^*} defined as the angle between the K direction in the K^* rest frame and the K^* direction in the B rest frame. We use an unbinned maximum likelihood fit to fit the two-decay angles simultaneously. Figure 5 shows the efficiency corrected angular distributions for the 39 observed $B \to \psi K^*$ events with the results of the fit overlaid. We find the longitudinal term dominates the rate

$$(\frac{\Gamma_L}{\Gamma})_{B\to\psi K^*} = 0.78 \pm 0.10 \pm 0.10 \quad . \tag{6}$$

The large amount of polarization suggests that this mode can be used to study CP violation.

4.2 $b \to s\gamma$

The *penguin* decay $b \to s\gamma$ would manifest in $B \to K^*\gamma$ final states. The theoretical predictions for exclusive $B \to K^*\gamma$ modes are not as reliable as the inclusive prediction for the $b \to s\gamma$ rate. The fact that the γ for all possible K^* channels falls within a narrow energy range, allows CLEO to search for an inclusive signal for $b \to s\gamma$. $B\overline{B}$ events are selected by cutting on the event shape, $R2 < 0.5$ [10]. We then search for isolated photons in the barrel portion of the calorimeter that fall within 2.2 GeV and 2.7 GeV in energy. This region has an efficiency of $85 \pm 5\%$ for the inclusive $b \to s\gamma$ rate. We take a conservative approach and use $\epsilon > 70\%$ when calculating upper limits. Continuum $q\overline{q}$ background is subtracted by using scaled continuum data. Figure 6 shows the continuum subtracted photon energy distribution for 507 pb^{-1} of data. The number of events within the signal region is 120 ± 55 photons. Outside the kinematical limit for photons from B decays, 3 GeV $< E_\gamma <$ 4 GeV, we observe 58 ± 47 photons, consistent with 0. We use the number of observed photons to set an upper limit on the inclusive $\mathcal{B}(b \to s\gamma)$ at $8.4 * 10^{-4}$ at the 90% confidence level. The current Standard Model prediction for inclusive $\mathcal{B}(b \to s\gamma)$ is $3 - 4 * 10^{-4}$.

4.3 $B^0 \to \pi^+\pi^-$ and $B^0 \to K^+\pi^-$

The search for the CP eigenstate, $B^0 \to \pi^+\pi^-$, is complicated by charged particle identification at high momentum. Since the B^0 is approximately at rest in the lab frame the π or K have approximately 2.6 GeV/c of momentum. The CLEO-II detector provides almost 2σ separation in dE/dx in this range. To discriminate among the four possible choices for the decay, $\pi^+\pi^-$, π^+K^-, $K^+\pi^-$ and K^+K^-, we form a χ^2 based on the energy loss measurements,

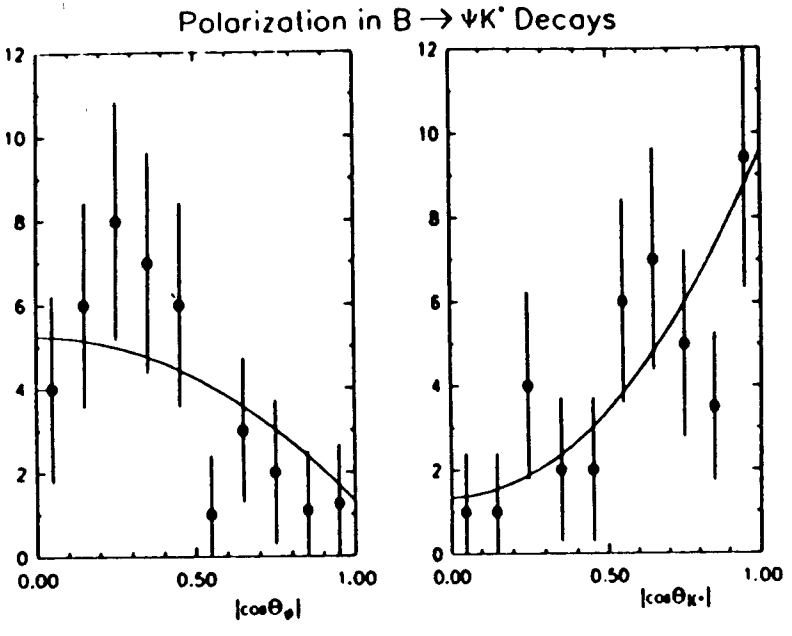

Figure 5: ψ and K^* decay angle distribution for $B \to \psi K^*$ decays. The overlaid smooth curves are projections of an unbinned maximum likelihood fit.

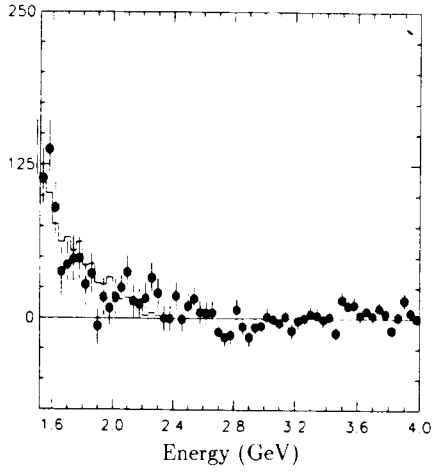

Figure 6: Photon yield as a function of energy after continuum subtraction. The signal region for $b \to s\gamma$ is between 2.2 and 2.7 GeV.

dE/dx. We calculate a χ^2 for each of the four hypotheses, for example the $K^+\pi^-$ χ^2 is as follows:

$$\chi^2_{K\pi} = \left(\frac{(dE/dx)_1 - (dE/dx)_K}{\sigma_{dE/dx}}\right)^2 + \left(\frac{(dE/dx)_2 - (dE/dx)_\pi}{\sigma_{dE/dx}}\right)^2. \qquad (7)$$

We then choose the hypothesis that has the highest probability, as long as it is greater than 10%. Monte Carlo studies show that we select the correct hypothesis 65% of the time. $K\pi$ combinations are misidentified as $\pi\pi$ combinations 9% of the time, and $K\pi$ combinations are misidentified 18% of the time.

In addition to particle assignments, we require that the event pass hadronic selection criteria and have at least five charged tracks. To reduce the amount of continuum background we cut on the angle, ψ, between the thrust axis of the candidate tracks and the thrust axis of the rest of the event. We require $|cos(\psi)| \leq 0.7$, neutral energy clusters with energy greater than 0.050 GeV are used in the event thrust axis determination. To further reduce the continuum background we use the candidate thrust axis, B flight direction, and variables describing the momentum flow of the event to form a Fisher discriminant. The Fisher discriminant had 85% efficiency for the signal events while rejecting 57% of the continuum background.

Figure 7 shows the beam constrained mass for those events that pass the cuts and are within $\pm 2\sigma$ of the beam energy for $B^0 \to \pi^+\pi^-$ and $B^0 \to K^+\pi^-$.

Decay Mode	Efficiency %	No. Events	Estimated Background	BR UL ($\times 10^{-5}$) at 90% CL This Result	Previous Result
$\pi^+\pi^-$	19 ± 3	4	1.2 ± 0.2	4.8	9 (Ref [12])
$K^+\pi^-$	19 ± 3	5	1.4 ± 0.4	5.6	9 (Ref [13])

Table 3: Preliminary upper limits B^0 branching ratios.

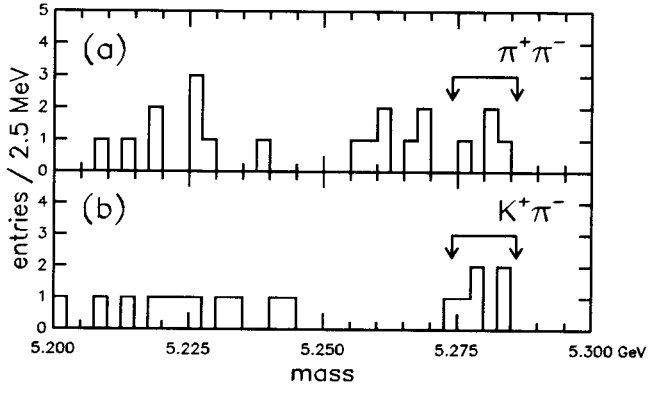

Figure 7: Beam constrained mass distribution for (a) $\pi^+\pi^-$ and (b) $K^+\pi^-$ candidates. The signal region is indicated by the arrows.

Figure 8 shows the ΔE distribution for events within $\pm 2\sigma$ of the B mass. We count 4 $\pi^+\pi^-$ events and 5 $K^+\pi^-$ events in the signal region. We estimate the background to be 1.2 ± 0.2 events for the $\pi^+\pi^-$ mode and 1.4 ± 0.2 for the $K^+\pi^-$ mode. The background is estimated from sidebands in ΔE and sidebands in the constrained B mass distributions. The upper limits obtained from the observed events is shown in Table 3. The upper limits obtained are smaller than previously obtained upper limits. The $\pi^+\pi^-$ upper limit is approaching theoretical predictions obtained with a value of $V_{ub} = 0.1$ [11].

5 Inclusive $\mathcal{B}(B \to Xl\nu)$ measurement

Since there isn't enough phase space for additional particles, the $\Upsilon(4S)$ decays into a $B\overline{B}$ pair. By reconstructing one of the B mesons the flavor of the other

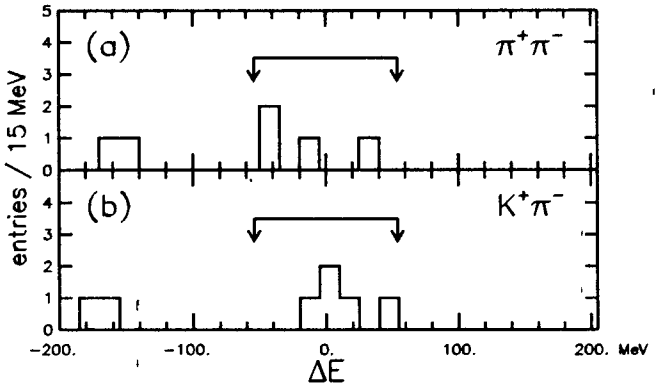

Figure 8: ΔE distribution for (a) $\pi^+\pi^-$ and (b) $K^+\pi^-$ candidates. The signal region is indicated by the arrows.

B is determined. In addition if one subtracts the tracks and showers that compose the tagged B, one is left with tracks and showers from an unbiased B partner meson. Using this tagging technique we measure the inclusive B semi-leptonic branching ratios by looking for leptons in a large sample of fully reconstructed B^+ and B^0 mesons.

To integrate as much as possible of the D and B meson branching fraction, we use the following D meson decays:

$$\begin{aligned} D^0 &\rightarrow K^-\pi^+ \\ &\rightarrow K^-\pi^+\pi^0 \\ &\rightarrow K^-\pi^+\pi^-\pi^+ \\ &\rightarrow K^0_s\pi^+\pi^- \quad , \end{aligned}$$

$$\begin{aligned} D^+ &\rightarrow K^-\pi^+\pi^+ \\ &\rightarrow K^0_s\pi^+ \\ &\rightarrow K^0_s\pi^+\pi^0 \\ &\rightarrow K^0_s\pi^+\pi^+\pi^- \quad , \end{aligned}$$

and the following D^* decays:

$$\begin{aligned} D^{*+} &\rightarrow D^0\pi^+ \\ &\rightarrow D^+\pi^0 \\ D^{*0} &\rightarrow D^0\pi^0. \end{aligned}$$

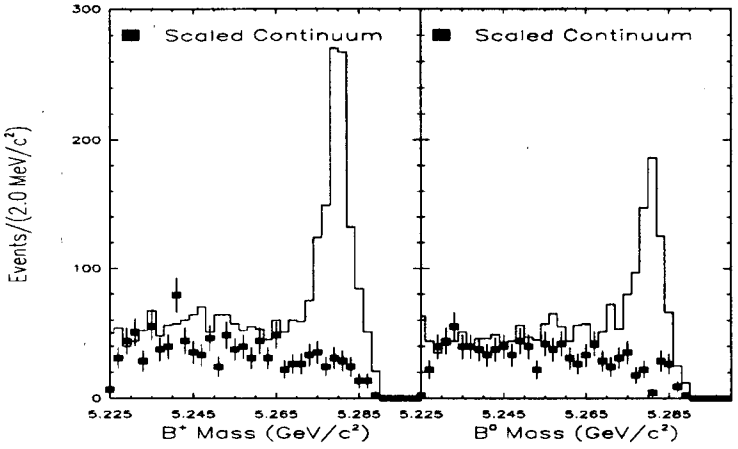

Figure 9: Beam constrained B^+ and B^0 mass distributions. The shaded squares represent the scaled continuum background.

The B mesons are then reconstructed in the following channels:

$$\begin{aligned} B &\rightarrow D\pi^\pm \\ &\rightarrow D^*\pi^\pm \\ &\rightarrow D\rho^\pm \\ &\rightarrow D^*\rho^\pm \\ &\rightarrow Da_1^\pm \\ &\rightarrow D^*a_1^\pm \quad . \end{aligned}$$

We also use the clean $B \rightarrow \psi K(or K^*)$ decays where the ψ decays into two leptons (electrons or muons). Figure 9 shows the beam constrained mass for charged and neutral B's. We find 601.5 ± 57.9 charged and 492.7 ± 43.6 neutral B mesons.

To obtain the inclusive semi-leptonic rates we now focus on the tracks left in the event once we subtract off the reconstructed B. Paying attention to lepton efficiencies and fake rates we obtain the yields in Table 4.

The overall efficiency for detecting leptons in the final state is model dependent. For this analysis we use the model of $ISGW$ and $ISGW^*$ to predict the lepton momentum spectra. Where $ISGW$ model assumes $B \rightarrow Dl\nu$ and $B \rightarrow D^*l\nu$ saturate the semi-leptonic width, and $ISGW^*$ assumes $B \rightarrow D^{**}l\nu = 26\%$ of the width [14]. The inclusive $\mathcal{B}(B \rightarrow Xl\nu)$ results are shown in Table 5 for the two different models. Since the lifetime is proportional to the inclusive semi-leptonic branching ratio, the ratio of the inclusive semi-

	Electrons	Muons	Fake Electrons	Fake Muons
B^+	96.2 ± 12.2	60.4 ± 8.6	7.6 ± 1.5	5.5 ± 1.7
B^0	60.1 ± 9.6	39.1 ± 6.9	4.1 ± 0.8	2.7 ± 0.8

Table 4: Efficiency (acceptance only) corrected lepton yields and fake yields.

	$ISGW(\%)$	$ISGW^*(\%)$
B^+	$12.0 \pm 2.2 \pm 1.3$	$12.8 \pm 2.3 \pm 1.4$
B^0	$10.8 \pm 2.1 \pm 1.4$	$11.5 \pm 2.3 \pm 1.4$

Table 5: Inclusive semi-leptonic branching ratios for the charged and neutral B mesons.

leptonic branching ratios is equal to the ratio of lifetimes, $\frac{\tau_{B^+}}{\tau_{B^0}} = \frac{\mathcal{B}(B^+ \to X l \nu)}{\mathcal{B}(B^0 \to X l \nu)}$. Using the results in Table 5 we obtain $\frac{\tau_{B^+}}{\tau_{B^0}} = 1.11 \pm 0.29 \pm 0.08$. The model dependency of this result is contained in the systematic error. This result is independent of the relative production cross section of charged and neutral B mesons. This result is in agreement with the previously measured ratio from the ratio of $\frac{\mathcal{B}(B^+ \to D^{*0} l^- \nu)}{\mathcal{B}(B^0 \to D^{*+} l^- \nu)}$ from CLEO [15] $\frac{\tau_{B^+}}{\tau_{B^0}} = (0.89 \pm 0.19 \pm 0.13)(f_0/f_+)$ and ARGUS [16] $\frac{\tau_{B^+}}{\tau_{B^0}} = (1.00 \pm 0.23 \pm 0.14)(f_0/f_+)$. Where f_0/f_+ is the ratio of B^0 to B^+ produced in $\Upsilon(4S)$ decays.

6 Conclusions

New results from the CLEO collaboration have been presented. The new upper limit on $\mathcal{B}(D^{*+} \to D^+ \gamma)$ differs from previous measurements of this branching ratio. The new value eliminates the need for a large anomalous magnetic moment for the charm quark. The new branching ratios measured for the D^* decays will scale previously measured $B \to D^* X$ branching ratios.

CLEO has searched for penguin decays of the B meson, and has set new lower upper limits for $B \to \pi^+\pi^-$, $B \to K^+\pi^-$, and $b \to s\gamma$ decays. Additional data and better understanding of the detector will aid these searches. New measurements of $B \to \psi K^{(*)}$ branching ratios were presented along with measurements of the polarization in the ψK^* decays. These measurements will help determine the luminosity requirements for studying CP violation in the B system.

An exhaustive effort to obtain a large sample for tagged B events has started to bear fruit with the exclusive semileptonic measurement of the B^+ and B^0 mesons. These tagged events with clean fully reconstructed B's represent a relatively new frontier in B physics, which we plan to exploit to its fullest potential.

7 Acknowledgements

The work presented here represents the efforts of the CLEO collaboration in operating the CLEO detector, processing the data and analyzing the data. Special thanks to the CESR staff for providing record luminosities and excellent running conditions.

References

[1] Y. Kubota *et al.*, Nucl. Intr. and Meth. **A320** (1992) 66.

[2] G. Goldhaber *et al.*, Phys. Lett. B **69**, 503 (1977);
Mark II Collaboration, M.W. Coles *et al.*, Phys. Rev. D **26**, 2190 (1982);
JADE Collaboration, W. Bartel *et al.*, Phys. Lett. B **161**, 197 (1985);
HRS Collaboration, E.H. Low *et al.*, Phys. Lett. B **183**, 232 (1987).

[3] Mark III Collaboration, J. Adler *et al.*, Phys. Lett. B **208**, 152 (1988).

[4] CLEO Collaboration, F. Butler, *et al.*, CLNS 92/1143 submitted to Phys. Rev. Lett. (1992).

[5] R. Brun, *et al.*, GEANT 3.14, CERN preprint CERN DD/EE/84-1.

[6] The error on the ratio is due to the error in the measured mass differences between, D^{*+} and D^0, and D^{*+} and D^+.

[7] Particle Data Group, M. Anguilar-Benitez *et al.*, Phys. Rev. D **45** Part 2 (1992).

[8] I. Dunietz *et al.*, Proceedings of the SLAC B-Factory Workshop, June 1990.

[9] M. Neubert, V. Rickert, Q. P. Xu and B. Stech, HD-THEP-91-28.

[10] G. Fox and S. Wolfram, Phys. Rev. Lett. **54**,381 (1985).

[11] L.-L. Chau *et al.*, Phys Rev **D43**, 2176 (1991).
N. G. Deshpande and J. Trampetic, Phys Rev. **D41**, 895 (1990).
M. B. Gavela *et al.*, Phys. Lett. **B154**, 425 (1985).

[12] CLEO Collaboration, P. Avery *et al.* , Phys. Lett. **B223**, 470 (1989).

[13] CLEO Collaboration, D. Bartoletto *et al.*, Phys. Rev. Lett. **62**, 2436 (1989).

[14] B. Grinstein and M.B. Wise, Phys. Lett. **B197** 249 (1987);
N. Isgur, D. Scora, B. Grinstein, and M. Wise, Phys. Rev. **D39** 799 (1989).

[15] CLEO Collaboration, R. Fulton *et al.*, Phys. Rev. **D43** 651 (1991).

[16] ARGUS Collaboration, H. Albrecht *et al.*, Phys. Rev. Lett. **B232** 554 (1989).